한국박용기관학회지 제27권, 제3호, pp. 421~428, 2003 (ISSN 1226-9549)
Journal of the Korean Society of Marine Engineers

Hysteretic Characteristics of Wells Turbine for Wave Energy Conversion

Tae-Hun Kim* · Yeon-Won Lee† · Yeong-Yeun Hwang**

(Manuscript : Received March 10, 2003 ; Revised April 8, 2003)

Key words : Wells Turbine, Hysteretic Characteristics, Wave Energy Conversion, Unsteady Flow

Abstract

The aerodynamic characteristics of the Wells turbine for wave energy conversion have been investigated by the numerical simulation to reproduce hysteretic behaviors. The pressure distributions on the suction surface of the blade were investigated to find out the cause of the hysteretic mechanism. The results have shown that the hysteretic behavior is associated with streamwise vortical flow appearing near the suction surface and become more obvious, as the tip clearance and solidity change . Also, it has shown that such phenomena occur due to different behaviors of wakes in the accelerating and decelerating flow process. The CFD analysis shows a good agreement with experimental results.

1. Introduction

Wave energy is one of the most important renewable resources. Considerable efforts have been devoted to the developments of ocean wave power conversion technology. The Wells turbine is one of the most suitable air turbine for wave energy conversion from oscillating air flow. So, it has been investigated and widely applied for ocean wave energy conversion, mainly due to its simple structure. In early researches[1-5], the design data and estimation of capacity of the Wells turbine

† Corresponding Author, (School of Mechanical Engineering, Pukyong National Univ.), E-mail : ywlee@pknu.ac.kr, T : 051) 620-1417
* Department of Mechanical Engineering, Graduated School of Pukyong National Univ.
** School of Electrical control and Instrumentation Engineering, Pukyong National Univ.

were obtained by the model turbine tests under steady flow conditions. However, Setoguchi reported the importance of unsteady flow characteristics in the Wells turbine[6]. The hysteretic characteristics of the Wells turbine cause inaccurate prediction of the turbine performance in a quasi-steady analysis, because it occurs in an unsteady state flow. of hysteresis, some experimental studies have been performed.[7,8]

They have scrutinized that the behaviors of dynamic stall and laminar separation bubble on the blade were not the cause of the hysteresis. Through the analysis of pressure distributions on the blade surface, it was found that the hysteresis occurred due to different behaviors of wakes between an accelerating flow and a decelerating flow. By the way, the CFD analysis has many advantages compared with the experiments. It is economical, flexible and possible to obtain a detailed insight of flow behaviors. In this paper, the CFD analysis was carried out to understand the detailed flow behaviors of the Wells turbine under the unsteady flow condition.

2. Numerical Method

2.1 Governing Equation

The three dimensional flow analysis of the Wells turbine in an unsteady state is performed by the Navier-Stokes equation and conservation equation of mass. And turbulent flow is modeled using the Renormalized Group (RNG) k-ε model with swirl modification and differential viscosity modeling.

Governing equations are as follows:

Continuity equation

$$\frac{\partial(\rho U_i)}{\partial X_i}=0 \tag{1}$$

Reynolds Averaged Navier-Stokes equation

$$\frac{\partial \rho U_j}{\partial t}+\frac{\partial(\rho U_i U_j)}{\partial X_i}=-\frac{\partial P}{\partial X_i}+ \frac{\partial}{\partial X_j}\left[\mu\left(\frac{\partial U_i}{\partial X_j}+\frac{\partial U_j}{\partial X_i}-\frac{2}{3}\sigma_{ij}\frac{\partial U_j}{\partial X_i}\right)\right]+\frac{\partial}{\partial X_j}\left(-\rho\overline{u_i u_j}\right) \tag{2}$$

Transport equation of turbulent kinetic energy, k

$$\frac{\partial(\rho k)}{\partial t}+\frac{\partial(\rho U_i k)}{\partial X_i}=\frac{\partial}{\partial X_i}\left[\left(\mu+\frac{\mu_i}{\sigma_k}\right)\frac{\partial k}{\partial X_i}\right] + \mu_t\frac{\partial U_j}{\partial X_i}\left(\frac{\partial U_i}{\partial X_j}+\frac{\partial U_j}{\partial X_i}\right)-\rho\varepsilon \tag{3}$$

Transport equation of the dissipation rate of turbulent kinetic energy, ε

$$\frac{\partial(\rho\varepsilon)}{\partial t}+\frac{\partial(\rho U_i\varepsilon)}{\partial X_i}=\frac{\partial}{\partial X_i}\left[\left(\mu+\frac{\mu_t}{\sigma_\varepsilon}\right)\frac{\partial \varepsilon}{\partial X_i}\right] + C_1\mu_t\frac{\varepsilon}{k}\frac{\partial U_i}{\partial X_j}\left(\frac{\partial U_i}{\partial X_j}+\frac{\partial U_j}{\partial X_i}\right)-C_2\frac{\rho\varepsilon^2}{k} \tag{4}$$

$$-\rho\overline{u_i u_j}=\mu_t\left(\frac{\partial U_i}{\partial X_j}+\frac{\partial U_j}{\partial X_i}\right)-\frac{2}{3}\rho k\delta_{ij} \tag{5}$$

Where ρ is the air density, U_i is the mean volocity in the X_i directions, P is the pressure, μ_t is the turbulent eddy viscosity, k is the turbulence kinetic energy, ε is the dissipation rate of the turbulence kinetic energy. $-\rho\overline{u_i u_j}$ is Reynolds stresses. The model constants are given as follows:

$C_\mu = 0.085,\ C_2 = 1.68,\ \sigma_k = 0.72,\ \sigma_\varepsilon = 0.72$

$C_1 = 1.42 - \eta(1-\eta/\eta_o)/(1+\beta\eta^3)$

$\beta = 0.012,\ \eta_o = 4.38,\ \eta = \frac{Sk}{\varepsilon},\ S = \sqrt{2S_{ij}S_{ij}}$

$S_{ij} = \frac{1}{2}\left(\frac{\partial u_i}{\partial x_j} + \frac{\partial u_j}{\partial x_i}\right)$

The turbulent viscosity can be calculated using the following relation.

$$\mu_t = C_\mu \rho \frac{k^2}{\varepsilon} \tag{6}$$

2.2 3-D unsteady state calculation

The 3-D computational data was based on the experimental data of the Wells turbine which were executed by Setoguchi in order to compare each other[11]. The computational conditions are tabulated in Table 1.

The 3-D grid system of the Wells turbine was generated for only one blade because of turbine geometry and its rotational characteristics. And the computational conditions were simplified by using periodic boundary conditions. The velocity of axial direction of the Wells turbine was modeled as a sinusoidal wave in this calculation. Therefore, Inlet boundary conditions were set at each time step. In order to apply the inlet boundary condition, the inlet velocity using a periodic function was generated as follows:

$$V = V_a(\sin 2\pi f t) \tag{7}$$

Where V_a is the highest speed of axial-direction, f is an oscillating number, t is time. Six seconds were set as one period.

Table 1 Computational Conditions.

Item	Conditions
Airfoil	NACA0021
Solidity	0.48, 0.57, 0.67
Number of blades	8
Tip clearance	1mm, 2mm, 3mm
Hub-to-tip ratio	0.7
Rotating speed	2000 RPM

In this study, obtained results during a half of one period were compared with experimental ones. A time step was set as 0.001 second in order to satisfy the CFL (Courant Friedrichs Lewy) condition. This condition proves the stabilization of the time marching computation. The governing

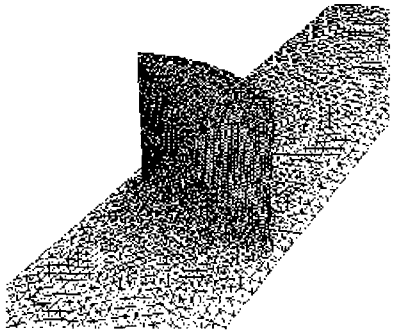

(a) Grid distributions

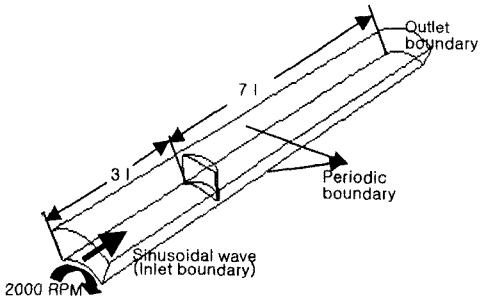

(b) Periodic domain

Fig. 2 Wells turbine geometry and boundary conditions.

equations have been solved using the Finite Volume Method. A Quick Scheme is used to calculate convective terms. The pressure and velocity components have been corrected in order to satisfy the continuity equation using the SIMPLE algorithm.[9] The numerical results of the flow simulation were affected by the grid parameters, i.e. grid distributions and number of grid points.

Figure 2 shows grid distributions and boundary conditions. Triangular grids are used on the surfaces of the blade and rotor axis. The number of grid points is approximately 240,000. More grid points are focused on the surface of the blade, because the flow on the surface of the blade can affect pressure distribution and hysteresis. No-slip boundary conditions were used on solid walls. The moving wall was used because of the rotating frame of reference. Periodic boundary conditions were used for the surfaces of circumferential sides. On the outlet boundary, the static pressures were set at each time step.

3. Results and discussion

Figure 3 shows the numerical results of hysteretic loops of the total pressure coefficient, C_A against the attack of angle in a half period of the sinusoidal flow with the change of Solidity and Tip clearance, respectively. The total pressure coefficient and attack of angle are defined as follows:

$$C_A = \Delta P_o Q / [(1/2)\rho(V_a^2 + U_R^2) z b l V a] \quad (8)$$

$$\alpha = \tan^{-1}\left(V_a / U_R\right) \quad (9)$$

where $\triangle P$. denotes the total pressure drop across the rotor, Q air flow rate, ρ density of air, Va axial velocity, Ur circumferential velocity at mid span, z number of blades, ℓ chord length. The angles of attack vary between 0° and maximum value(15°) in the phase of oscillating flow. In the course of the cyclic loop, the value of C_A during the acceleration of the axial velocity is lower than one during deceleration. So an counterclockwise hysteretic loop appears as shown in this figure. This hysteretic characteristics in a reciprocating flow was found in the experiment.[7,8].

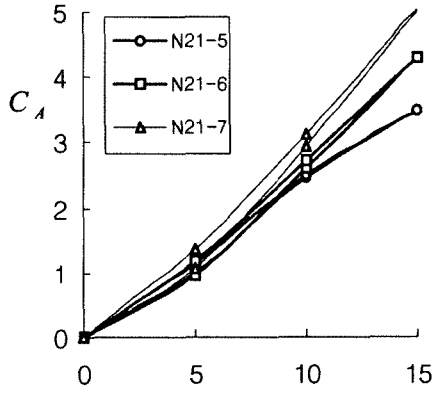

(a) Solidity

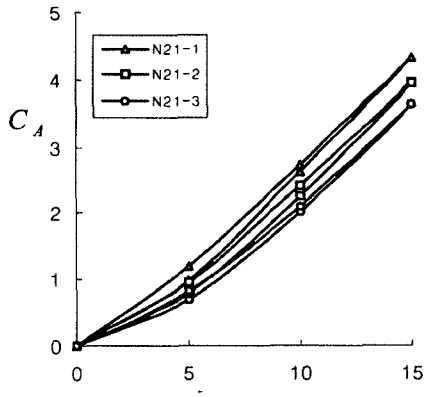

(b) Tip clearance

Fig. 3 Hysteresis loops for the total pressure coefficient (C_A).

And these results become more apparent as the tip clearance decreases and the solidity increases.

If this hysteretic behavior is the same phenomena occurring due to the dynamic stall of an airfoil, a clockwise hysteretic loop should be observed.[4]

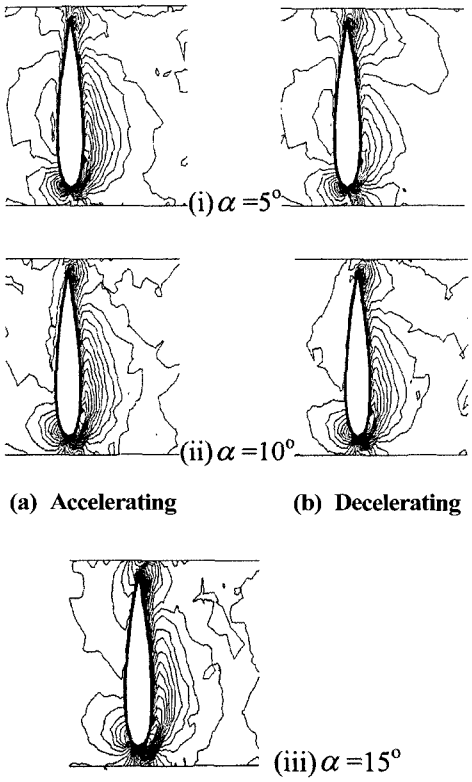

(a) Accelerating (b) Decelerating

Fig. 4 Relative velocity contours at the mid-span(NACA21-7-1).

Kim et al[12] revealed that the dynamic stall in the Wells turbine would be reproduced in a numerical simulation using the k-ε turbulence model when the angle of attack approach to 30°. Therefore, the mechanism of hysteretic behavior of the Wells turbine is different from that of the dynamic stall of the airfoil. It is thought that the hysteresis occur due to the different behavior of wake flows between an increasing process and a decreasing process in the angle of attack.

Figure 4 and 5 show relative velocity contours at the mid-span of NACA21-7-1 (z=7, tip clearance=1mm) and NACA21-6-1 (z=6, tip clearance=1mm) respectively

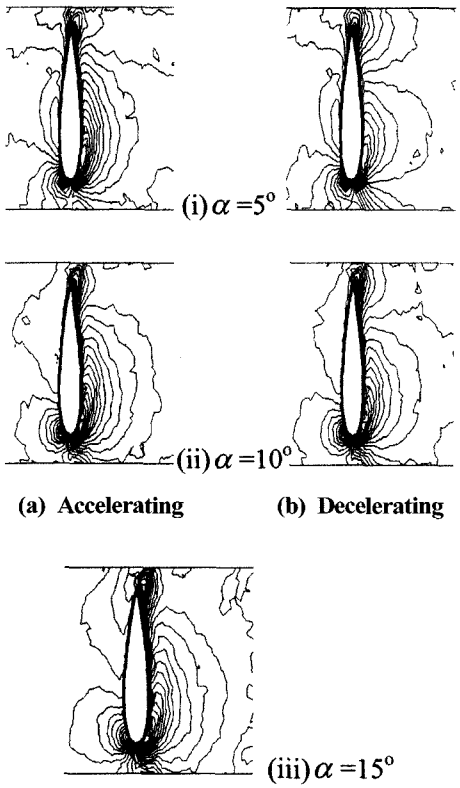

(a) Accelerating (b) Decelerating

Fig. 5 Relative velocity contours at the mid-span (NACA21-6-1).

when the angle of attack changes from 0° to 15°. The contours of axial velocities around suction surfaces in the decelerating process are different from those in the accelerating process. In particular, the differences near the leading edge and trailing edge of blades are so evident. This result describes that the wake flow occurred near the trailing edge

has an influence on the suction surface of the next blade. It is an evidence that the behavior of this wake cause hysteretic characteristics. Also these results are more obvious when solidity increases as shown in fig. 3.

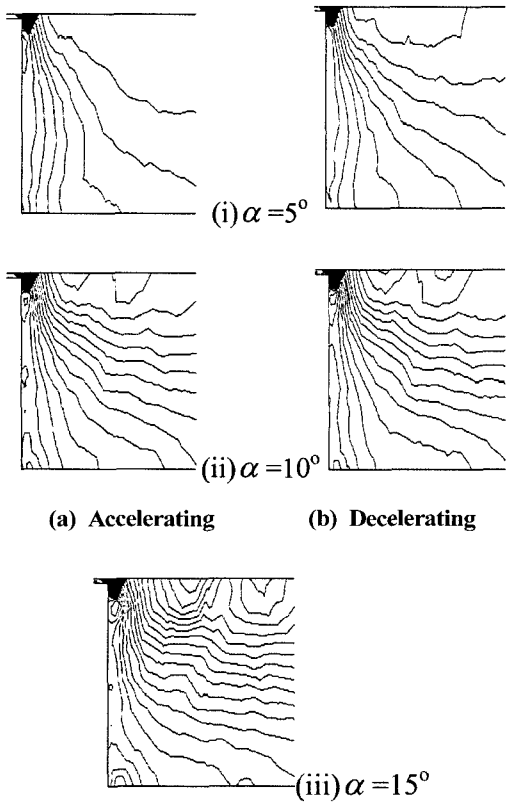

(a) Accelerating **(b) Decelerating**

Fig. 6 Velocity contours of axial direction in mid-chord (NACA21-6-1).

Figure 6 shows the velocity contours of the axial direction in the mid-chord. The velocity contours passing through the tip are very dense. In the previous study, It was found that the vortex motion occurred near the tip because of relatively high speed in comparision with the hub. This has an effect on the velocity contours of the suction side. Thus, the pattern of axial velocity contours at the suction side shows a little difference between the accelerating process and the decelerating process. This result is another evidence that cause the hysteretic characteristics of the Wells turbine.

Figure 7 shows the axial velocity vectors projected on the planes perpendicular to the rotating axis in the accelerating and decelerating processes. The vortex motion is generated throughout the gap of the tip and the wakes occurred around the trailing edge interact in the suction side of blades.

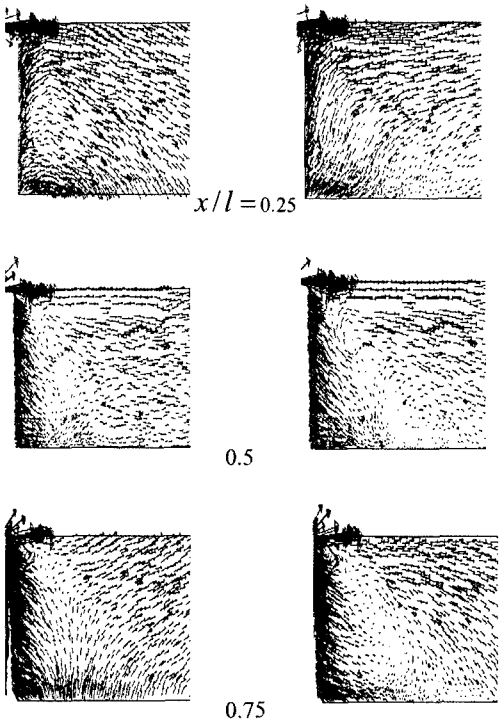

(a) Increasing **(b) Decreasing**

Fig. 7 Velocity vectors projected on the plane perpendicular to the rotating axis(NACA21-6-1).

The wake flow in the suction side becomes very complicated by this interaction and the different patterns around the suction side are found during the two processes.

As mentioned before, these reasons make the hysteretic loops of the total pressure coefficient as shown in fig. 3.

4. Conclusion

Numerical analysis using using the RNG k-ε turbulence model was accomplished in order to obtain the unsteady flow characteristics of the Wells turbine operated under a reciprocating flow. The CFD analysis shows a good agreement with experimental results.

1) The count-clockwise loops of the total pressure coefficient are well reproduced. This hysteretic characteristics occur due to the different behavior of wake flows between the increasing process and decreasing process in the angle of attack. These results become more apparent as the tip clearance decreases and the solidity increases.

2) The tip vortex motion is generated near the tip and the wakes occurred around the trailing edge and rotor blade interact in the suction side. As a result, The wake flow in the suction side becomes very complicated by this interaction and the different flow patterns around the suction side appear during the two processes.

5. REFERENCE

[1] T. Setoguchi, M. Takao, K. kaneko, 1998, "Hysteresis on Wells Turbine Characteristics in Reciprocating Flow "Journal of rotating machinery Vol. 4 No1 pp 17 ~ 24.

[2] Patankar, Suhas V., Numerical Heat Transfer and Fluid Flow , Hemisphere Publishing Corporation, United States of America, 1980

[3] K. Kaneko, T. Setoguchi and M. Inoue, 1987, Hysteretic characteristics of wells turbine in reciprocating flow , J. of The Flow Visualization Society of Japan (in Japanese), 7(26), 153-156

[4] Ericsson, L.E. and Reding, J.P.,1987, Fluid Dynamics of Unsteady Separated Flow, Part II. Lifting Surfaces, Progress in Aerospace Science, Vol. 24, 249-356

[5] J. H. Kim, H. G. Lee, Y. W. Lee, Y. H. Lee and T. Setoguchi, A Study on Flow Characteristics of a Wells Turbine for Wave Power Conversion Using Numerical Analysis, The Korean Society of Marine Engineers, Vol. 25, January 1. 2001.

[6] A. Thakker, S. Slater, A Study of CFD Air flow Prediction in a Wells turbine , International Offshore and Polar Engineering Conference May 24~29. 1998.

[7] A. Thakker, P. Frawley and E. Sheik Bajeet, Numerical Analysis of Wells Turbine Performance Using a 3-D Navier Stokes Explicit Solver Proceedings of the ISOPE, Stavanger, Norway, June 17-22, 2001.

[8] Falcao, A.F.O., Whittaker, T.J.T. and Lewis, A.W.(1993)JOULE II Preliminary Action : European Wave Energy Symp., pp 247 ~ 257

[9] H. G. Lee, J. H. Kim, Y. W. Lee, T. Setoguchi and C. S. Kang, Numerical Analysis of Flow Charactersitcs in a Wells Turbine for Wave Power Conversion , International Offshore and Polar Engineering Conference (ISOPE),

May 28-June2, 20.

[10] J. K. Waterson, S. Raghunathan, Inversigation of Wessl turbine Performance Using 3-D CFD, IEEE, 1996.

[11] J. K. Waterson, S. Raghnathan, Computed Effects of Tip Clearance On Wells Turbine Performance , AIAA, January 6-10, 1997

[12] Mueller, T. J., 1985, The influence of laminar separation and transition low Reynolds number airfoil hysteresis . J. Aircraft, 22(9), 763-770.

[13] T. Setoguchi, K. Kenoko, H. Hamakawa and M. Inoue, Hysteretic Characteritics of the Biplane Wells Turbine in a Reciprocating Flow , JSME (B), Vol. 55, No. 512, pp 1153~1158, 1989.

저 자 소 개

이연원 (李蓮源)

1958년 8월생, 1981년 경북대학교 기계공학과졸업. 1983년 경북대학교 대학원 기계공학과 졸업(석사), 1993년 일본 동경대학 대학원 기계공학과 졸업(박사). 1984년-1986년 현, POSCO E&C 설계팀장, 1997년 7월 - 8월 일본 동경대학 생산기술연구소 객원연구원, 1993년 - 현재 부경대학교 기계공학부 부교수, 당학회 종신회원

황용연 (黃龍淵)

1959년 5월생. 1982년 인하대학교(기계공학전공) 졸업. 1989년 일본요꼬하마국립대학 대학원 박사과정전기 졸업(석사). 1992년 동대학원 박사과정후기 졸업(박사). 1992년~현재 부경대학교 전기·제어계측공학부 부교수. 당학회 회원.